Int. J. Electrochem. Sci., 8 **(2013)** 887 - 902

International Journal of
ELECTROCHEMICAL
SCIENCE
www.electrochemsci.org

The Electrochemical Characteristics of Cr30Mo2 Ultra Pure Ferritic Stainless Steel in NaCl Solutions at Different Temperatures

Xin Wei[1,2], *Junhua Dong*[1,*], *Jian Tong*[1], *Zhi Zheng*[1], *Wei Ke*[1]

[1] State Key Laboratory for Corrosion and Protection, Institute of Metal Research, Chinese Academy of Sciences, Shenyang 110016, China
[2] College of Materials Science and Engineering, Dalian University of Technology, Dalian 116024，China
[*]E-mail: jhdong@imr.ac.cn

Received: 8 November 2012 / *Accepted:* 4 December 2012 / *Published:* 1 January 2013

The electrochemical characteristics of Cr30Mo2 ultra pure ferritic stainless steel in 0.01-2 M NaCl solutions at different temperatures (25-90 °C) had been investigated using different electrochemical techniques of potentiodynamic polarization, electrochemical impedance spectroscopy, capacitance measurements (Mott–Schottky approach) and potentiostatic polarization measurements. The results revealed that the pitting corrosion behavior of this stainless steel was found to be dependant on the temperature and chloride concentration of the solution. As the temperature and Cl^- concentration were increased, the pitting potentials of the stainless steel shifted to negative direction, the impedances of passive films decreased and the donor densities (N_D) in oxide films calculated from the Mott-Schottky plots increased in the range of 1.6 - 7 × 10^{21} cm^{-3}. Besides, the incubation time of pitting corrosion of Cr30Mo2 stainless steel shortened with the increase of temperature. Combining with micrographs of pits, it was recognized that the pitting corrosion resistance of Cr30Mo2 stainless steel declined in the concentrated NaCl solution at higher temperature.

Keywords: ferritic stainless steel, pitting corrosion, passive film, temperature

1. INTRODUCTION

In many severe corrosion environments, both ferritic stainless steel and austenitic stainless steel could exhibit excellent uniform corrosion resistance due to their abilities in forming self-engendered protective oxide film. Nevertheless, the cost of ferritic stainless steel is relatively low for free of alloy element Ni, and ferritic stainless steel are gradually inclining to substitute austenitic stainless steel in some fields such as nuclear power industry, petroleum chemistry, desalination of sea water, coastal

roof materials, etc. [1-4]. But, conventional ferritic stainless steels still have some weakness and flaws especially in ductility and toughness of welded joints are much inferior to those of austenitic stainless steels [5-8], which have strictly limited the applications of conventional ferritic stainless steels. However, since the end of the 20th century, the great progress of ultra-low carbon and nitrogen refining techniques have assisted some steel company successfully developed qualified ultra purity grades ferritic stainless steels ($w_{[C+N]} \leq 150\times10^{-6}$). Ultra purity Cr18Mo2, Cr26Mol and Cr30Mo2 grades stainless steels have exhibited lower embrittlement transition temperatures than their conventional grades [5, 9-11]. Besides, the most important concern for high chromium ferritic stainless steels is its localized corrosion resistant performance, which mainly depends on the steel composition, especially the amount of carbon, nitrogen and molybdenum [12-17]. Yoshioka et al. [5] indicated that the intergranular corrosion resistance of high Cr-Mo ferritic stainless steels can be evidently improved by reducing C and N contents to extremely low levels. Moreover, reducing the impurity level of 11Cr and 30Cr-2Mo ferritic stainless steels was found to be beneficial to decrease the donor density in the passive oxide film of n-type semiconductor [14]. Bond [15] and Kaneko [16] pointed out that the addition of Mo could improve the pitting potentials of common and high purity ferritic stainless steels of Fe-18%Cr-x%Mo in both chloride and bromide solutions. Hashimoto et al. [17] showed that the passive current density of 30Cr-2Mo ferritic stainless steel is two orders of magnitude lower than that of 30Cr steel without Mo in 1 M HCl. Besides, the susceptibility of localized corrosion of stainless steel strongly depends on the environmental factors such as temperature, pH and the concentration of aggressive species (such as chloride ion). A lot of studies have been devoted to investigate the effects of temperature and Cl^- concentration on the localized corrosion for stainless steels [18-33]. It is generally recognized that the localized corrosion takes place when the temperature and the concentration of chloride ion exceed a threshold value, and the critical condition is responsible for the breakdown of the passive film.

Normally, the localized corrosion of passive metal is an electrochemical process, and the nucleation as well as propagation of localized corrosion is strongly correlated to the electrochemical characteristics of the passive film. Therefore, it is necessary to investigate the electrochemical behaviors of the passive films formed in different environments to further understand the resistance to localized corrosion for stainless steels. Electrochemical measurements, such as electrochemical impedance spectroscopy, cyclic polarization, capacitance measurements and X-ray photoelectron spectroscopy [34-37], have showed that the temperature and solution concentration had relatively greater effect on the composition, structure and electronic properties of the passive film formed on stainless steel [34, 35]. The point defect model (PDM) has proved that the key parameters for passive film growth are the diffusivity and density of the defects, which varied with the corrosion environment [38]. Our previous study has shown that Cr26Mo1 ultra pure ferrite stainless steel has an excellent resistance to pitting corrosion in 0.6 M NaCl solution at 25 °C. While the protective properties of the passive film become weak and the susceptibility of pitting corrosion remarkably increases when the temperature was above 45 °C [39]. However, few works for studying the electrochemical behaviors of the ultra pure high chromium ferritic stainless steel (Cr30Mo2) were carried out.

The present work aims to investigate the effects of temperature and Cl^- concentration on the electrochemical behaviors and the protective properties of the passive film on Cr30Mo2 ultra pure

ferrite stainless steel in NaCl solution by different electrochemical techniques to understand the electrochemical characteristics and critical conditions, and to evaluate the resistance of Cr30Mo2 stainless steel to pitting corrosion in a rigorous environments.

2. EXPERIMENTAL

2.1. Samples and test solution preparation

The material used in this work is ultra pure ferritic stainless steel (Cr30Mo2), with the chemical compositions (wt. %): C 0.0028, N 0.0028, Cr 31.5， Mo 2， Nb 0.15 and remainder Fe. The specimens were cut into 10mm×10mm×10mm pieces which were ground with SiC papers subsequently to 800 grits and then cleaned with ethanol and deionized water prior to test. The test mediums used in experiments were NaCl solutions with different concentration， which were prepared by the analytical-grade reagents and distilled water. All the measurements were carried out under open to air conditions in the temperature range of 25-90 °C.

2.2. Electrochemical measurements

Electrochemical experiments were carried out using a Princeton Applied Research 2273 Advanced Electrochemical System. A conventional three-electrode cell was used for the experiments. The working electrode was embeded in epoxy resin with 1 cm^2 test area exposing to the test solution, and the counter electrode was a Pt foil, and the reference electrode SCE connected to a Luggin capillary with a salt bridge.

Electrochemical measurements were started after stabilizating the electrode system for about 30 minutes at open-circuit potential (OCP). The Electrochemical impedance spectroscopy (EIS) measurements were carried out in the frequency range from 100 kHz to 10 mHz with a signal amplitude perturbation of 10 mV. All the impedance data were fitted with the ZSimpWin 3.10 software. The potentiodynamic polarization was carried out to obtain the corrosion potential, the pitting potential and passive current density. The scan rate was 0.33 mVs^{-1}. The pitting potential was defined as the potential where pit-growth occurred at a current density of more than 100 μAcm^{-2} in forward scan. The capacitance measurements were performed on the films at a frequency of 1000 Hz in the potential range -0.6 V to 0.8 V (SCE) using a 10mV AC signal and a step rate of 20 mV. The Cyclic polarization curves were carried out to further understand the susceptibility of the pitting corrosion of Cr30Mo2 stainless steel. The specimens were polished with W1.5 diamond polishing paste. Scanning direction was reversed when the current density respectively arrived at a limited threshold value of 10^{-4}, 10^{-3} and 10^{-2} Acm^{-2}. The scan rate was 0.5 mVs^{-1}. Microscopic examination was also performed by using an optical microscope to investigate the effects of temperature and Cl^- concentration on the surface morphology of the film after anodic polarization. The potentiostatic polarization experiments were carried out at applied anodic potential of 500 mV (SCE) to measure the

variation of current density with time in order to determine the incubation times of pitting corrosion at various constant temperatures.

3. RESULTS AND DISCUSSION

3.1 Potentiodynamic measurements

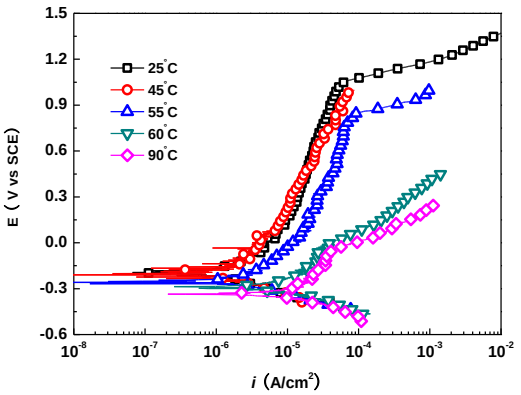

Figure 1. Potentiodynamic polarization curves of Cr30Mo2 ultra pure ferrite stainless steel in 0.6 M NaCl solution at different temperatures

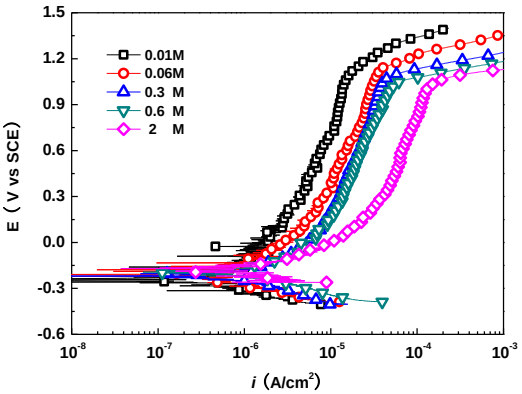

Figure 2. Potentiodynamic polarization curves of Cr30Mo2 ultra pure ferrite stainless steel in NaCl solutions with different concentration at 25 °C

Fig.1 shows the effect of temperature (25-90 °C) on the polarization curves of Cr30Mo2 stainless steel in 0.6 M NaCl solution. It indicates that, with increasing the temperature, the corrosion potential shifts to less noble and the corrosion current density increases. From 25 to 55 °C, the polarization curves exhibit a wider passive potential region. However, when the temperature increases to 60 and 90 °C, the passive potential region shrinks and the pitting potential decreases which can be attributed to the degradation of the protective property and the stability of the passive film at higher

temperature. In addition, due to H_2O and O_2 are prone to adsorb on film at lower temperature, the concentration of dissolved oxygen and oxygen reduction rate decrease with increasing temperature. Accordingly, the pH values decrease in some localized micro-regions, which finally results in the breakdown of passive film.

It is well known that the passive film is susceptible to be localized breakdown in the presence of chloride ions. Figure 2 presents the concentration effect of NaCl solution on the polarization curves of Cr30Mo2 stainless steel at 25 °C. All the polarization curves exhibit the typical passive characteristics. With increasing Cl^- concentration, the passive current density increases and the pitting corrosion potential decreases. These results are attributed to the probability of Cl^- colliding on the oxide film rising with the increase of Cl^- concentration. Furthermore, Cl^- and cation are combined to form the soluble halide which can accelerate the occurrence of pitting corrosion [32]. Therefore the pitting corrosion of Cr30Mo2 is prone to occur in NaCl solution with higher Cl^- concentration.

3.2 Electrochemical impedance spectroscopy

Table 1. Fitting results of the equivalent circuit of Cr30Mo2 ultra pure ferrite stainless steel in 0.6 M NaCl solution at different temperatures (25-90 °C)

T ℃	R_s Ω·cm^2	Q_1 F·cm^2	n_1	R_f Ω·cm^2	Q_2 F·cm^2	n_2	R_p Ω·cm^2
25	6.523	9.46×10^{-5}	0.87	743.7	2.05×10^{-4}	0.71	57050
45	3.792	1.13×10^{-4}	0.86	604.9	8.51×10^{-5}	0.72	23520
60	1.761	1.16×10^{-4}	0.89	154.4	3.07×10^{-4}	0.57	5002
90	0.773	6.997×10^{-5}	0.8	11.13	4.9×10^{-4}	0.8	3868

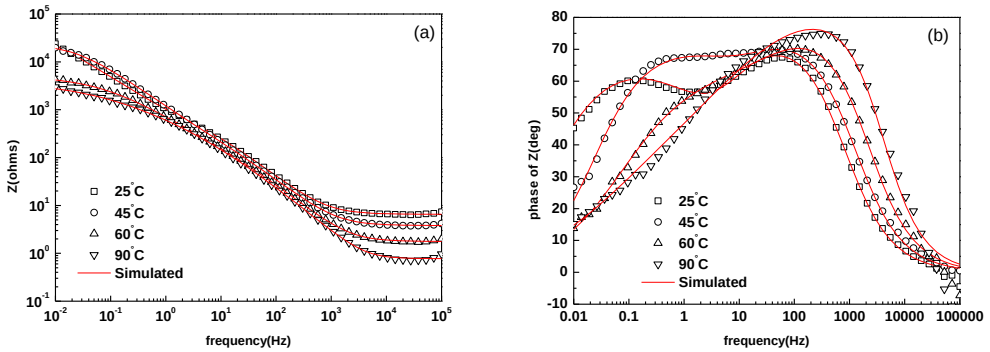

Figure 3. Bode plots of Cr30Mo2 ultra pure ferrite stainless steel in 0.6 M NaCl solution at different temperatures (25-90 °C): (a) impedance modulus (b) phase angle

Fig.3 presents the Bode plots of Cr30Mo2 ultra pure ferrite stainless steel in 0.6 M NaCl solution at 25, 45, 60 and 90 °C. In the extremely high-frequency region, the impedance modulus corresponding to the solution resistance R_s increases with increasing temperature. In the extremely

low-frequency area, the impedance modulus corresponding to the polarization resistance R_p decreases almost one order of magnitude when the temperature exceeds 60 °C, which indicates a degradation of the corrosion resistance of Cr30Mo2 ultra pure ferrite stainless steel. Moreover, all phase angle exhibit two peaks which shift toward high frequency region with increasing temperature. Usually, the feature for two relaxation time constants is considered as the response of an inhomogeneous film, which composed of the substrate and a porous outer layer. Table1 lists the fitted parameters according to the equivalent circuit of $R_s\{Q_1[R_f(Q_2R_p)]\}$ for simulating the EIS shown in Fig.3 [40-42]. Where R_s is the solution resistance, Q_1 is the capacitive behavior of the passive film, R_f is the passive film resistance, Q_2 is the capacitive behavior at the interfaces, and R_p is the polarization resistance. Table 1 indicates that all R_s, R_f and R_p decrease with increasing temperature, which can be attributed to the increase of electric conductivity and Cl^- activity.

Table 2. Fitting results of the equivalent circuit of Cr30Mo2 passive films in NaCl solutions with different Cl^- concentrations (0.01-2 M) at 25 °C

C mol/L	R_s $\Omega\cdot cm^2$	Q_1 $F\cdot cm^2$	n_1	R_f $\Omega\cdot cm^2$	Q_2 $F\cdot cm^2$	n_2	R_p $\Omega\cdot cm^2$
0.01	281.9	9.205×10^{-5}	0.83	5490	2.06×10^{-4}	0.54	4.21×10^{5}
0.06	47.22	1.14×10^{-4}	0.82	3450	1.81×10^{-4}	0.64	8.4×10^{4}
0.6	6.523	9.46×10^{-5}	0.87	743.7	2.05×10^{-4}	0.71	5.7×10^{4}
2	2.85	4.171×10^{-5}	0.97	8.8	3.08×10^{-4}	0.56	5.5×10^{3}

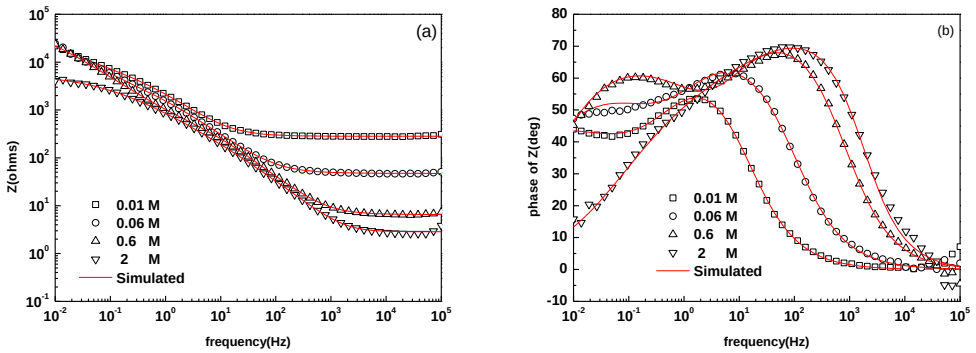

Figure 4. Bode plots of Cr30Mo2 ultra pure ferrite stainless steel in NaCl solutions with different Cl^- concentrations (0.01-2 M) at 25 °C: (a) impedance modulus (b) phase angle

Fig.4 presents Bode plots for Cr30Mo2 ultra pure ferrite stainless steel in NaCl solutions with different Cl^- concentrations (0.01-2 M) at 25 °C. In the high-frequency region, R_s decrease with increasing Cl^- concentration. In the low-frequency area, most of the R_p are almost same in 0.01-0.6 M NaCl solutions, but it evidently decreases in 2 M NaCl solution. The phase angles move to high frequency direction with increasing Cl^- concentration. In order to further understand the effect of chloride concentration on the EIS of Cr30Mo2 ultra pure ferrite stainless steel, the equivalent circuit R_s

$\{Q_1 [R_f (Q_2 R_p)]\}$ was also used to fit the relevant parameters of EIS shown in Fig.4. The fitting results indicate (table2) that R_s, R_f and R_p all decrease with increasing chloride concentration. Therefore, there is a lower resistance to corrosion of passive film in solution with higher chloride concentration.

3.3 Semiconductor properties of passive films

Usually, the passive film of ferrite stainless steel is considered to be composed of iron and chromium oxide and to have the semiconductive properties, and its capacitance property can reflect the electronic property of the films formed on the Cr30Mo2 stainless steel in different environments [43-45]. The Mott-Schottky relationship involves the apparent capacitance measurement as a function of potential under depletion condition [46, 47]:

n-type: $$\frac{1}{C^2} = \frac{2}{\varepsilon\varepsilon_0 e N_D}(E - E_{fb} - \frac{kT}{e}) \quad (1)$$

p-type: $$\frac{1}{C^2} = -\frac{2}{\varepsilon\varepsilon_0 e N_A}(E - E_{fb} - \frac{kT}{e}) \quad (2)$$

Where C is the capacitance of the space charge region, E is the applied potential, ε is the dielectric constant of the semiconductor, ε_0 is the permittivity of free space, N_D is the donor density in the oxide film, N_A is the acceptor density in the oxide film, E_{fb} is the flatband potential, k is the Boltzmann constant and T is the temperature. According to the Mott-Schottky equation, C^{-2} versus E plots describes the semiconductor type of the passive film.

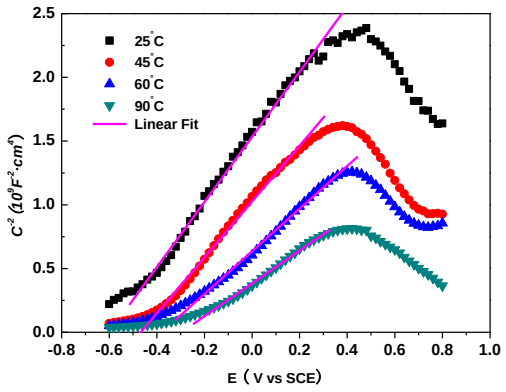

Figure 5. The Mott-Schottky curves for the passive films formed on Cr30Mo2 ultra pure ferrite stainless steel in 0.6 M NaCl solution at different temperatures (25-90 °C)

Fig. 5 shows the C^{-2} versus E curves obtained for the oxide films formed on Cr30Mo2 ultra pure ferrite stainless steel, at temperatures between 25 and 90 °C. The Mott-Schottky curves reveal a linear relationship between C^{-2} and E. When potential is below 0.4 V (SCE), the slope is positive indicating a n-type semiconductor, After that the slope changes to a negative slope indicating a p-type

semiconductor. In addition, the Mott-schottky plots show a transition from n-type to p-type semiconductor. From the slope of the straight line of the C^{-2} versus E curves, the donor densities of the Fe and Cr oxide layers formed at the different temperatures can be calculated using ε = 12. The values of N_D are subsequently as 3.5×10^{21}, 4.1×10^{21}, 5.4×10^{21} and 7.0×10^{21} cm^{-3} for the different temperatures (25-90 °C), which indicates the donor density increases with the rise of temperature for the film formation.

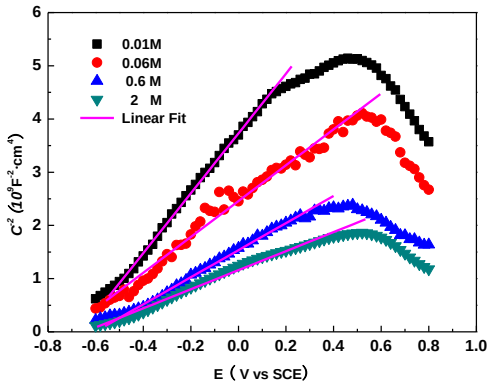

Figure 6. The Mott-Schottky curves for the passive films formed on Cr30Mo2 ultra pure ferrite stainless steel in NaCl solutions with different Cl^- concentrations (0.01-2 M) at 25 °C

Fig.6 shows the Mott-Schottky plots for the passive films formed on Cr30Mo2 ultra pure ferrite stainless steel in different concentrations of NaCl solution at 25 °C. The slope decreases with increasing the concentration of NaCl, which is correlated with the non-uniform donor distribution within the film. Based on the Mott-Schottky equation, the calculated donor densities are subsequently as 1.6×10^{21}, 2.7×10^{21}, 3.5×10^{21} and 5.0×10^{21} cm^{-3} in 0.01-2 M NaCl solutions. N_D in passive film formed in concentrated solution is more than dilute solution at 25 °C. The results are consistent with other reports [35, 38, 48].

According to the point defects model (PDM) [49-52], the donors or acceptors in semiconducting passive films are defects themselves including cation vacancies, anion vacancies and metal interstitials. Both anion vacancies (oxygen vacancy) and metal interstitials (Cr^{2+}, Cr^{3+} and Fe^{2+}) in the metal/film interface play the role of electron donors, and metal vacancies in the film/solution interface play the role of acceptors. At the initiation of pitting corrosion, the main reaction that occurs at the film/solution interface involves the adsorption of Cl^- into the oxygen vacancies, followed by a Schottky pair type reaction. Many cation vacancies are generated at the film/solution interface after Cl^- migrate through the passive film to the film/metal interface, and then oxygen vacancies and cation interstitials transport from the metal/film interface to the film/solution interface. If the amount of cation vacancies is so excessive that it cannot be compensated by the generation of cation interstitials, cation vacancy condensates are formed. When the condensates grow to a critical size, the pitting corrosion occurs. From Figs.5 and 6, the higher values of N_D obtained in solutions with higher Cl^- concentration and temperature, which related to the increase of the number of point defects within the film formed on Cr30Mo2 ultra pure ferrite stainless steel. Moreover, both temperature and Cl^- can

accelerate the diffusion of the defects within the passive film [35, 36]. Therefore, the resistance to pitting corrosion of Cr30Mo2 ultra pure ferrite stainless steel decreased with increasing temperature and Cl^- concentration.

3.4 Pitting susceptibility

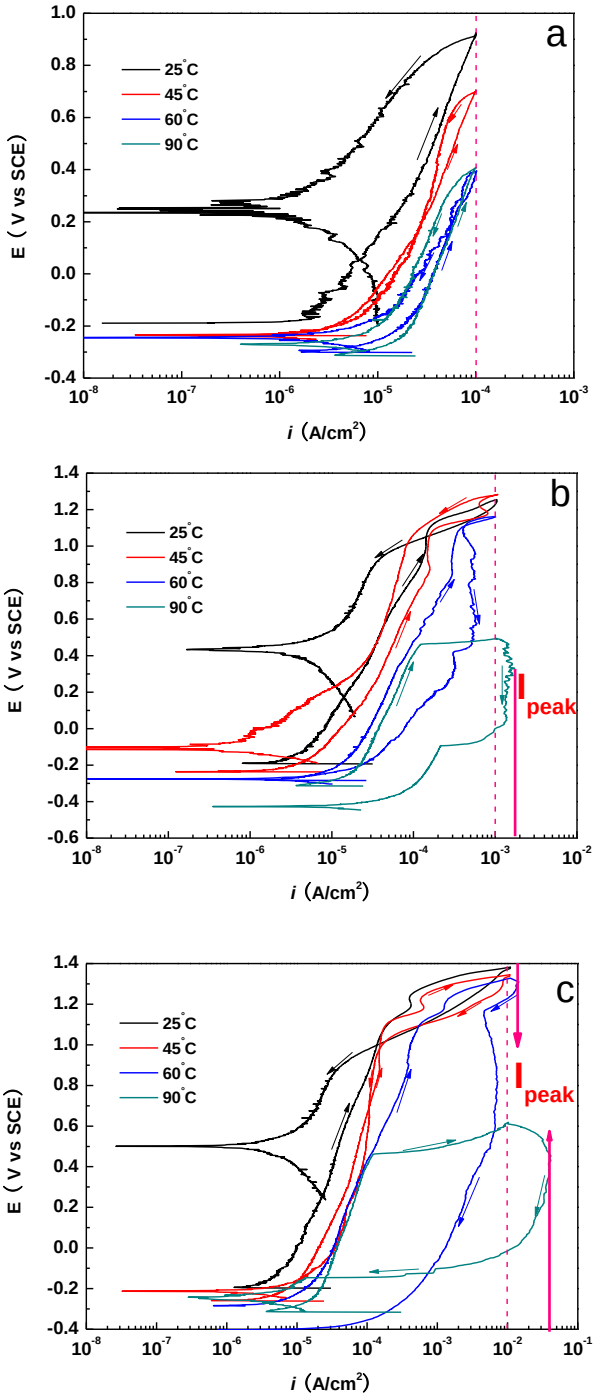

Figure 7. Cyclic polarization curves of Cr30Mo2 ultra pure ferrite stainless steel in 0.6 M NaCl solution at different temperatures. (The reverse scan starts at (a) 10^{-4} A/cm^2 (b) 10^{-3} A/cm^2 (c) 10^{-2} A/cm^2). The scan rate was 0.5 mV/s.

Fig. 7 shows the cyclic polarization curves of Cr30Mo2 ultra pure ferrite stainless steel in 0.6M NaCl solution at 25-90 °C. The reverse scan starts at the current density (a) 10^{-4} A/cm^2 (b) 10^{-3} A/cm^2 (c) 10^{-2} A/cm^2. Fig.7 (a) shows that all cyclic polarization curves do not have a hysteresis loop at 25-90 °C when the reverse scan starts at 10^{-4} A/cm^2. The forward scan current densities are higher than backwards at the same potential, indicating the good stability and self-repairing ability of the passive film. From Fig.7 (b), the hysteresis loop does not appear on the cyclic polarization curves until the temperature exceeds 45 °C, and the area of the hysteresis loop increases with increasing temperature. When the temperature is 90 °C, the current density of the reverse scan continuously increases and finally reaches to a maximum value (1.7 mA) in the potential range of 0.4 to 0 V (SCE). It indicates that the stabilization and the self-repair ability of the passive film of Cr30Mo2 ultra pure ferrite stainless steel decreased with increasing temperature when the reverse scan starts at 10^{-3} A/cm^2. Fig.7(c) shows that all the cyclic polarization curves have a hysteresis loop at 25-90 °C when the reverse scan starts at 10^{-2} A/cm^2, indicating a delay in repassivation of the existed pits. In addition, the maximum current densities (I_{max}) attained on the reverse scan curves at 60 and 90 °C have reached to 14 and 43 mA, respectively, which can be ascribed to the self-catalytic effect of the deep corrosion pits caused by the higher reverse current density. Therefore temperature plays an important role to promote the ionic activities of Cl^-, which decreases the pitting corrosion resistance and self-repair ability of the passive film [53-55]. For the pitting specimens, it can not be self-repaired as before.

The cyclic polarization curves of Cr30Mo2 ultra pure ferrite stainless steel in different NaCl solutions (0.01- 2 M) at 25 °C are shown in Fig.8. When the reverse scan starts at 10^{-4} A/cm^2, the cyclic polarization curves shown in Fig.8 (a) shows that the forward scan current densities are lower than the reverse current density in NaCl solutions (0.01-2 M). Nevertheless, a hysteresis loop is observed in all the cyclic polarization curves when the reverse scan starts at 10^{-3} and 10^{-2} A/cm^2, which is shown in Fig.8 (b) and (c), respectively. Furthermore, all the maximum values of current density are appeared on the reverse scan curves in 2 M NaCl solution, which are 2.2 and 13.8 mA/cm^2 respectively relation to the reverse current densities of 10^{-3} and 10^{-2} A/cm^2. According to the obtained results in above, we can draw the conclusion that the pitting corrosion susceptibility of Cr30Mo2 ultra pure ferrite stainless steel increases with increasing the chloride concentration at 25 °C.

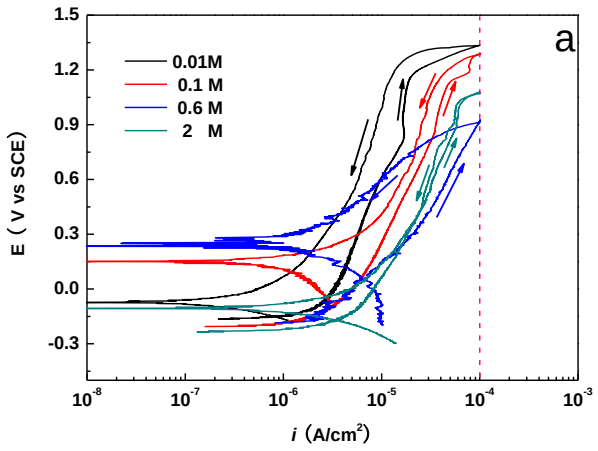

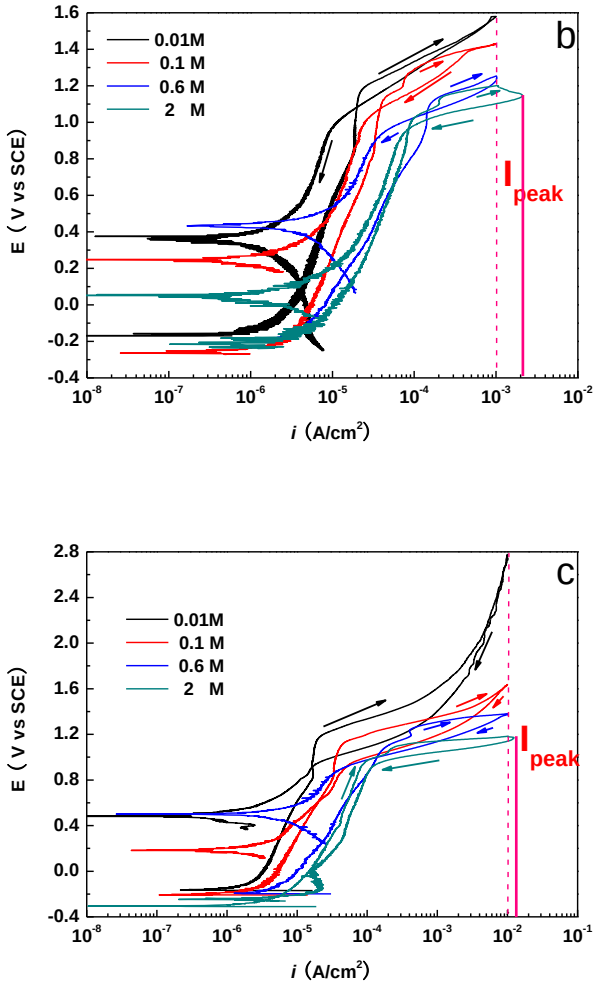

Figure 8. Cyclic polarization curves of Cr30Mo2 ultra pure ferrite stainless steel in solutions with different concentration of NaCl at 25 °C (0.01-2 M). (The scan direction reversed when the current density respectively arrived at (a) 10^{-4} A/cm^2 (b) 10^{-3} A/cm^2 (c) 10^{-2} A/cm^2). The scan rate was 0.5 mV/s.

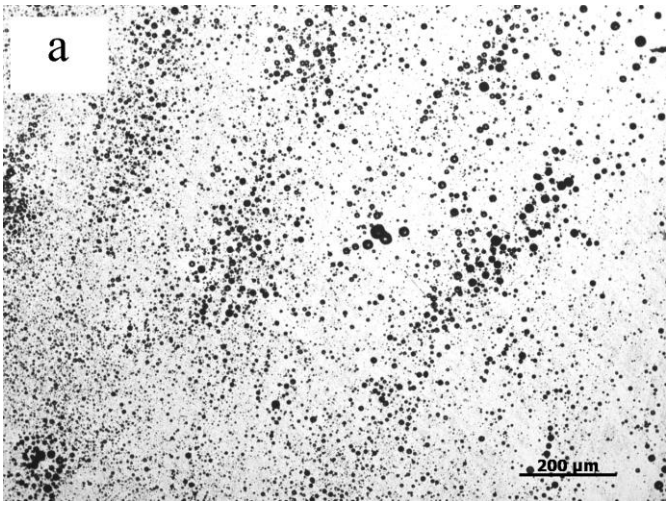

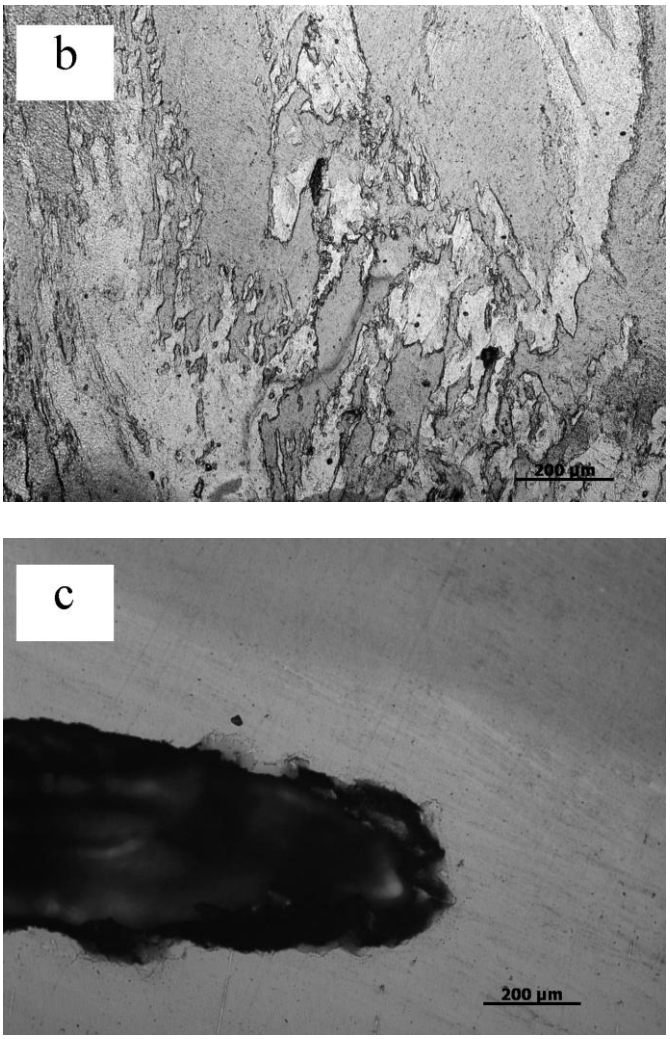

Figure 9. Optical micrographs of Cr30Mo2 ultra pure ferrite stainless steel after polarized (the current density arrived at 10^{-2} A/cm^2) shows the degree of pitting damage to specimens: (a) 0.6 M NaCl 25 °C (b) 2 M NaCl 25 °C (c) 0.6 M NaCl 90 °C.

Fig.9 shows the Optical micrographs of Cr30Mo2 ultra pure ferrite stainless steel after polarized in different environments when the current densities arrive at 10^{-2} A/cm^2. Fig.9 (a) presents a high density of corroded micro-pits on the surface of the stainless steel in 0.6 M NaCl at 25 °C, which indicates the uniform distribution of cumulate damage on the passive film. In 2 M NaCl solution, the passive film is severely dissolved and accompanied with some corrosion pits at 25 °C (as shown in Fig.9 (b)). Comparing with Fig.9 (a), the number of pits reduces obviously whereas the size of pits increases. It can be found that the primary corrosion mechanism in 2 M NaCl solution is anodic dissolution coming with the pitting corrosion at 25 °C. Fig.9 (c) exhibits only one big corrosion pit on the passive film although the rest of film remains passivation, which is caused by the self-catalytic effect at higher temperature. The breakdown of passive film is mainly caused by the localized acidification and enrichment of chloride ions within the pit. The results further illustrate that the susceptibility of localized corrosion of Cr30Mo2 ultra pure ferrite stainless steel strongly depends on the environment factors such as temperature and chloride concentrations.

3.5 The incubation time of pitting corrosion

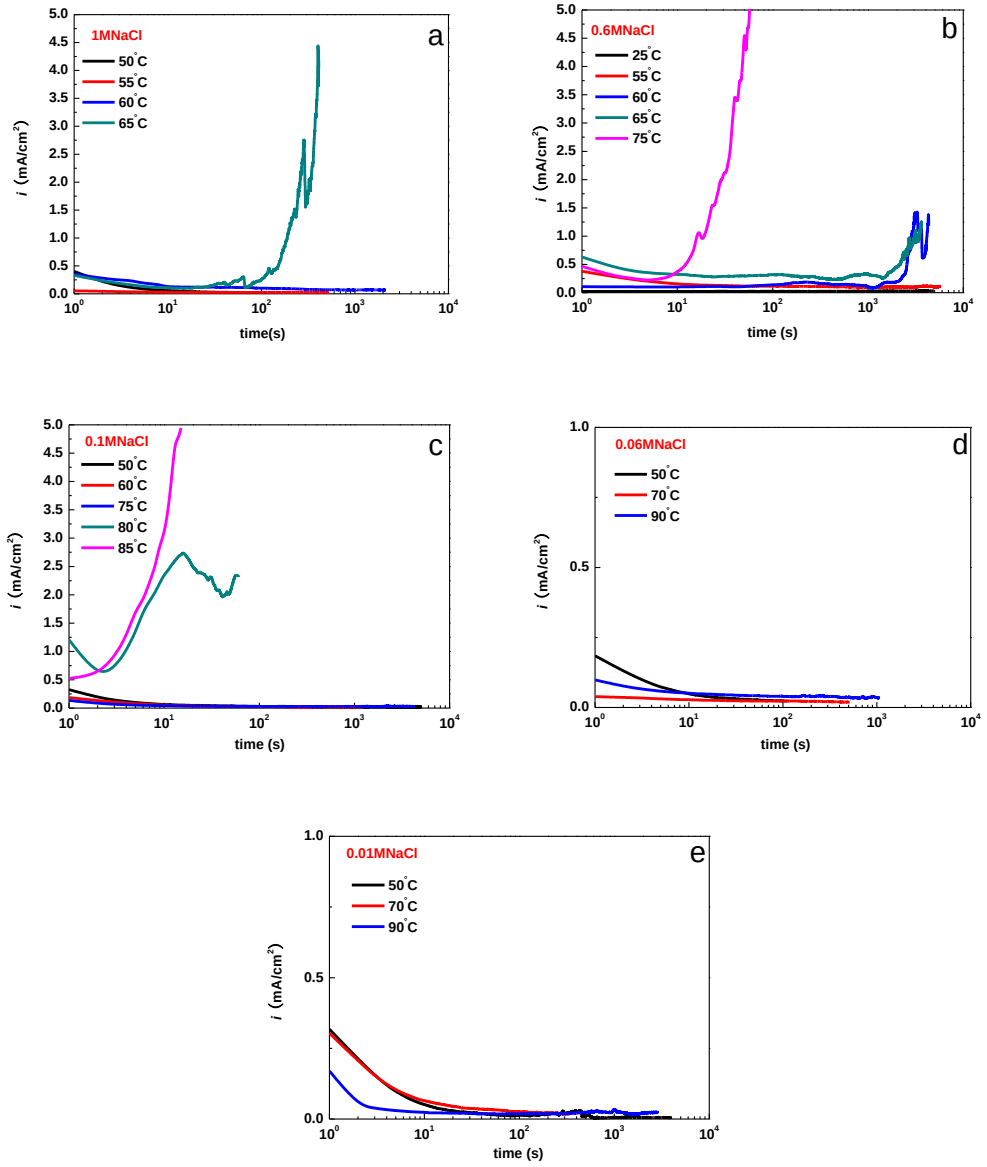

Figure 10. Potentiostatic polarization results with applying 500 mV (SCE) anodic potential for Cr30Mo2 ultra pure ferrite stainless steel at different temperatures in NaCl solutions: (a) 1 M (b) 0.6 M (c) 0.1 M (d) 0.06 M (e) 0.01 M

In general, pitting corrosion of stainless steel spends an incubation time from initiation to penetration, and the incubation time of pitting corrosion strongly depends on the environmental factors. Fig.10 shows the potentiostatic polarization results for Cr30Mo2 ultra pure ferrite stainless steel with applying 500 mV (SCE) anodic potential in 0.01-1 M NaCl solutions at different temperatures. From Fig.10 (a), the current density increases quickly at 65 °C in 1M NaCl solution and the incubation time is about 69 seconds. However, the current density keeps an extremely small value even in 3600 s when the temperature is lower than 60 °C. Fig.10 (b) shows that the current density in

0.6 M NaCl solution decreases and keeps a lower value at 55 °C. However, when the temperature increases to 60 °C, the current density quickly reaches to 1.4 mA/cm^2 after 2052 s, and decreases instantly. The fluctuation of current density on the curve can be associated to the metastable development and formation of pits on the surface of Cr30Mo2 ultra pure ferrite stainless steel at 60 °C. When the temperatures increase to 65 and 75 °C, the incubation times of pitting corrosion are respectively shorten to 1470 and 8 s. From Fig.10(c), all the current densities at 50-75 °C decrease and keep an extremely small value in 3600 seconds in 0.1 M NaCl solution. At 80 and 85 °C, the incubation times of pitting corrosion are respectively 3 and 1 s. Fig.10 (d) and (e) respectively show the current densities for Cr30Mo2 ultra pure ferrite stainless steel in 0.06 and 0.01 M NaCl solutions. The current densities decrease gradually and remain extremely small values in 3600 s even at 90 °C. The results suggest that the incubation time of pitting corrosion shortens with increasing temperature in the same concentration of NaCl solution. And also, at a constant temperature, the incubation time becomes short with increasing chloride concentration.

Summary on the results of experiments above indicates that the pitting corrosion resistance of Cr30Mo2 ultra pure ferrite stainless steel is better than AISI 304 and 316L austenitic stainless steel in hot solutions with Chloride [4, 18, 26], which make it a possible substitute for the more expensive austenitic stainless steel.

4. CONCLUSIONS

Based on the results attained by various electrochemical techniques for Cr30Mo2 ultra pure ferrite stainless steel, conclusions are summarized as below:

(1) The pitting potential and the resistance of the oxide film decrease with increasing temperature and/or chloride concentrations, while the passive current density as well as the donor densities values (N_D) increase with increasing temperature and/or chloride concentrations.

(2) The area of the hysteresis loop in cyclic polarization curves increases with increasing temperature, chloride concentrations and reverse current density, which means that these factors would accelerate the breakdown of the passive film and increase the susceptibility of the pitting corrosion. As for the pitting specimens, they can not be self-repaired as before.

(3) The incubation time of the pitting corrosion is shortened with increasing temperature in NaCl solution with the same chloride concentration, and the critical temperature of pitting corrosion declines in concentrated NaCl solution.

ACKNOWLEDGEMENTS
The authors gratefully acknowledge the financial support from the National Natural Science Foundation of China (No.51071160)

References

1. G. O. Ilevbare, G. T. Burstein, *Corros Sci.*, 45 (2003) 1545
2. I. Sekine, C. Okano, M. Yuasa, *Corros Sci.*, 30 (1990) 351
3. T. Ujiro, S. Satoh, R. W. Staehle, W. H. Smyrl, *Corros. Sci.*, 43 (2001) 2185
4. T.Bellezze, G.Roventi, A.Quaranta, R. Fratesi, Mater. *Corros.*, 59 (2008) 27

5. K. Yoshioka, S. Suzuki, N. Kinoshita, T. Hirano, Y. Hirose, M. Kurosawa, *Kawasaki steel tech. rep.*, 3 (1986) 101
6. K. F. Krysial, *Weld. J.*, 65 (1986) 37
7. D. H. Kah, D. W. Dickinson, *Weld. J.*, 60 (1981) 135
8. W. O. Binder, *Trans ASM*, 43 (1951) 759
9. H. Katayama, H. Kajioka, M. Inatomi, F. Tanaka, H. Hosoda, *Trans ISIJ*, 18 (1978) 761
10. X. M. You, Z. H. Jiang, H. B. Li, J. iron steel res. int., 14 (2007) 24
11. T. Kishida, H. Ushiyama**,** H**.** Hasegawa, T. Yajima, *Scand J. Metallurgy*, 22 (1993) 173
12. J. D. Gate, R. A. Jago, *Mater. Sci. Tech.*, 3 (1987) 450
13. J. Shu, H. Y. Bi, X. Li, Z. Xu, *Corros. Sci.*, 57 (2012) 89
14. M. Abe, A. Hyono, M. Ueda, T. Ohtsuka, T. Ishii, *J. Electrochem. Soc.*, 2 (2012) 2118
15. P. Bond, *J. Electrochem. Soc.*, 120 (1973) 603
16. M. Kaneko, H. S. Isaacs, *Corros. Sci.*, 44 (2002) 1825
17. K. Hashimoto, K. Asami, A. Kawashima, H. Habazaki, E. Akiyama, *Corros. Sci.*, 49 (2007) 42
18. P. Ernst, R.C. Newman. *Corros. Sci.*, 49 (2007) 3705
19. I. L. Rosenfeld, I. S. Danilov, R. N. Oranskaya, *J. Electrochem. Soc.*, 125 (1978) 1728
20. L. Stockert, F. Hunkeler, H. Bohni, *Corros.*, 41 (1985) 676
21. H. P. Leckie, H. H. Uhlig, *J. Electrochem. Soc.*, 113 (1966) 1262
22. V. Hospadaruk, J.V. Petrocelli, *J. Electrochem. Soc.*, 113 (1966) 878
23. N. D. Stolia, *Corros. Sci.*, 9(1969) 455
24. M. Kaneko a, H.S. Isaacs, *Corros. Sci.*, 44 (2002) 1825
25. M. A. Streicher, *Corros.*, 30 (1974) 77
26. J. O. Park, S. Matsch, H. Böhni, *J. Electrochem. Soc.*, 149 (2002) B34
27. I. L. Rosenfeld, I. S. Danilov, R. N. Oranskaya, *J. Electrochem. Soc.*, 125 (1978) 1728.
28. G. O. Ilevbare, G. T. Burstein, *Corros. Sci.*, 45 (2003) 1545
29. M. H. Moayed, R. C. Newman, *Corros. Sci.*, 48 (2006) 1004
30. R. J. Brigham, E. W. Tozer, *Corros. Sci.*, 29 (1973) 33
31. R. Qvarfort, *Corros. Sci.*, 29 (1989) 987
32. M. H. Moayed, R. C. Newman, *Corros. Sci.*, 48 (2006) 1004
33. J. R. Galvele, *Corros. Sci.*, 21 (1981) 551
34. A. Fattah-alhosseini, M. A. Golozar, A. Saatchi, K. Raeissi, *Corros. Sci.*, 52 (2010) 205
35. A. M. P. Simoes, M. G. S. Ferreira, G. Lorang，M. da Cunha Belo, *Electrochim. Acta*, 36 (1991) 315
36. S. Ahmad, A. U. Malik, *J. Appl. Electrochem.*, 31 (2001) 1009
37. L. Freire, M. J. Carmezima, M. G. S. Ferreira, *Electrochim. Acta*, 55 (2010) 6174
38. E. Sikora, J. Sikora, D. D. Macdonald, *Electrochim. Acta*, 41 (1996) 783
39. X. Wei, J. H. Dong, J. Tong, Z. Zheng, W. Kei. *Acta Metall. Sin.*, 48 (2012) 502
40. H. Luo, C. F. Dong, X. G. Li, K. Xiao, *Electrochim. Acta*, 64 (2012) 211
41. A. Kocijan, D. K. Merl, M. Jenko, *Corros. Sci.*, 53 (2011) 776
42. B. Guitián, X. R. Nóvoa, B. Puga, *Electrochim. Acta*, 56 (2011) 7772
43. M. J. Carmezim, A. M. Simoes, M. F. Montemor, M. Da CunhaBelo, *Corros. Sci.*, 47 (2005) 581
44. M. G. S. Ferreira, N. E. Hakiki, G. Goodlet, S. Faty, A. M. P. Simoes, M. Da Cunha Belo, *Electrochim. Acta*, 46 (2001) 3767
45. E. Mc Cafferty, *Corros. Sci.*, 45 (2003) 301
46. B. Jin, M. S. Zheng, J. W. Zhu, *Corros. Sci. Prot. Technol.*, 18 (2006) 348
47. Y. H. Lin, R. G. Du, R. G. Hu, C. J. Lin, *Acta Phys. Chim. Sin.*, 21 (2005) 740
48. S.J. Ahn, H.S. Kwon, *Electrochim. Acta*, 41 (2004) 3347–3351.
49. D. D. Macdonald, M. Urquidi-Macdonald. *J. Electrochem. Soc.*, 137 (1990) 2395
50. D. D. Macdonald, *J. Electrochem. Soc.*, 153 (2006) B213
51. D. D. Macdonald, *J. Nucl. Mater.*, 379 (2008) 24

52. A. Shahryari, S. Omanovic. *Electrochem. Commun.*, 9 (2007) 76
53. C. N. Cao. *Principles of Electrochemistry of Corrosion*, Chemical Industry Press, Beijing, China, 2008, p. 248
54. F. Eghbali, M. H. Moayed, A. Davoodi, N. Ebrahimi, *Corros. Sci.*, 53 (2011) 513
55. S. Ningshen, U. K. Mudali, V. K. Mittal, H. S. Khatak, *Corros. Sci.*, 49 (2007) 481